Available online at www.sciencedirect.com

SciVerse ScienceDirect

Ceramics International 39 (2013) 7439–7444

CERAMICS INTERNATIONAL

www.elsevier.com/locate/ceramint

One-dimensional ZnO nanostructure growth prepared by thermal evaporation on different substrates: Ultraviolet emission as a function of size and dimensionality

N.K. Hassan[a,b,*], M.R. Hashim[a], M. Bououdina[c]

[a]*Nano-Optoelectronics Research Laboratory, School of Physics, Universiti Sains Malaysia, 11800 Penang, Malaysia*
[b]*Department of Physics, College of Education, Tikrit University, Tikrit, Iraq*
[c]*Nanotechnology Centre, University of Bahrain, P.O. Box 32038, Bahrain*

Received 8 February 2013; accepted 25 February 2013
Available online 7 March 2013

Abstract

Large-scale uniform one-dimensional ZnO nanostructures were fabricated through thermal evaporation via the vapor solid mechanism on different substrates. The effects of Si (100), Si (111), SiO_2 and sapphire substrates with constant oxygen treatment on the morphology and diameter of ZnO nanostructures were investigated. It is found that the type of substrate has a great effect on the shape and diameter of the synthesized nanowires, nanorods, and nanotubes. It is noticed that the size and dimensionality were the most influential parameters on both structural and optical properties of the grown ZnO nanostructures. X-ray diffraction analysis confirms the stability of the wurtzite crystal structure for all grown ZnO nanostructures and the preferred orientation is substrate dependent. The crystallinity as well as the defects within the crystal lattice of the grown ZnO nanostructures was studied through Raman spectroscopy. The photoluminescence spectra of ZnO nanostructures grown on Si (100), Si (111), SiO_2 and sapphire substrates showed two peaks at a near-band-edge (NBE) emission in the ultraviolet region and a broad deep-level emission (DLE) around the green emission.
© 2012 Elsevier Ltd and Techna Group S.r.l. All rights reserved.

Keywords: One-dimensional ZnO; Catalyst free; Large scale; UV emission enhancement

1. Introduction

Nanoscale one-dimensional (1D) ZnO has received particular attention owing to its distinguished performance in sensing [1,2] and optoelectronics [3–6] applications. The enhancement of the optical properties results from the increase in radiative recombination, which depends on the size and dimensionality of the nanostructure [7].

Due to the electron confinement properties of 1D nanostructure, the polar nature which has been found in (1D), the direct wide band gap of 3.37 eV at room temperature and large excitation binding energy of 60 meV, ZnO becomes one of the most important functional components in the fabrication of optoelectronic devices. Well aligned 1D ZnO nanostructures have been applied to ultra-violet (UV) detectors working at room temperature and to improve their performance and its sensitivity to UV illumination.

Numerous efforts have been devoted to fabricate 1D ZnO nanostructures via various methods such as sol–gel [8], chemical vapor deposition (CVD) [9,10] sputtering [11,12], pulsed laser deposition (PLD) [13] and vapor-phase transport process [14–18]. The vapor process is one of the most important approaches to growing aligned and uniform ZnO with a variety of nanostructures such as nanowires, nanorods, and nanotubes, which offer a broad range of technological applications.

The synthesis of ZnO through this method has several advantages over the other methods, including mainly high crystallinity, controlled size and dimensionality of 1D nanostructures and morphology. Thereby, ZnO has been introduced as an attractive material in optoelectronic applications, in which 1D nanomaterial plays an important

*Corresponding author. Tel.: +60 17 8820803.
E-mail address: nadeemkhalid1969@yahoo.com (N.K. Hassan).

0272-8842/$ - see front matter © 2012 Elsevier Ltd and Techna Group S.r.l. All rights reserved.
http://dx.doi.org/10.1016/j.ceramint.2013.02.088

role in achieving the main objective of such devices. In the vapor process, many researchers have deposited ZnO on metal-coated substrates such as gold, which is used as a catalyst, this technique is called vapor liquid solid (VLS) [13,14] method. Alternatively, numerous studies in the literature have shown that it is possible to synthesize various ZnO-based nanostructures without the need of catalysts; this method is called catalyst-free vapor process (VS) [16–22].

The aim of this study is to fabricate a large-scale 1D ZnO using a low-cost technique, as well as to identify the most suitable substrate for the development of aligned, uniform 1D ZnO nanostructures grown via VS, which would be a potential candidate for UV detector. The experimental results demonstrate that both size and dimensionality are most probably responsible for the structural and optical properties of the grown ZnO nanostructures. The fabricated 1D ZnO UV-detector showed a significantly different response for the UV illumination which depends on size and dimensionality.

2. Experimental part

1D ZnO nanostructures were synthesized on Si (100), Si (111), SiO_2 and sapphire substrates, in a horizontal tube furnace system without using a metal catalyst. The experimental setup consisted of a three-zone tube furnace with a removable thermocouple, a quartz tube with a diameter of 12 cm and a length of 120 cm with 70 cm reaction zone and a gas flow-rate controller. A small quartz tube closed from one end and measuring 25 cm and 2 cm in length and diameter, respectively, was placed inside the large tube to confine the high-concentration of Zn vapor. High purity Zn powder (99.999%; Sigma-Aldrich) was used as the source material, which was placed in a quartz boat. This boat was then inserted inside the small tube near the closed end. The substrates were placed downstream of the Zn material. The small tube containing the Zn material and the substrate were inserted into the center of the furnace. The source material of Zn and the substrate were gradually heated up to 900 °C from room temperature at a rate of 10 °C/min. High-purity N_2 gas was fed at a rate of about 0.2 l/min. Oxygen gas was not fed into the furnace until 5 min after the temperature reached 900 °C. The oxygen gas flow rate was kept at 0.05 l/min and was fed into the reaction for 90 min. White material was formed on the substrate afterwards.

Morphological observations of 1D ZnO nanostructures were carried out using a scanning electron microscope (SEM) JEOL model JSM-6460LV, which was installed with energy dispersive X-ray spectroscopy. Structure analysis was studied using an X-ray diffractometer PANalytical X'Pert PRO diffractometer equipped with Cu-Kα radiation ($\lambda = 1.5418$ Å). The photoluminescence (PL) spectra of the samples were measured using a He–Cd laser (325 nm) at room temperature. Raman spectrum was obtained using a Raman spectrometer (Horiba Jobin Yuon HR800) operating at a wavelength of 514.55 nm using Ar^+ as the excitation source.

3. Results and discussion

3.1. Morphological study

SEM images depicting the evolution of the morphology of ZnO grown on different substrates, namely Si (100), Si (111), SiO_2 and sapphire, are shown in Fig. 1. The 1D ZnO nanostructures were successfully fabricated through the thermal evaporation of metal Zn grains via the VS method. The effect of substrate with constant oxygen treatment at

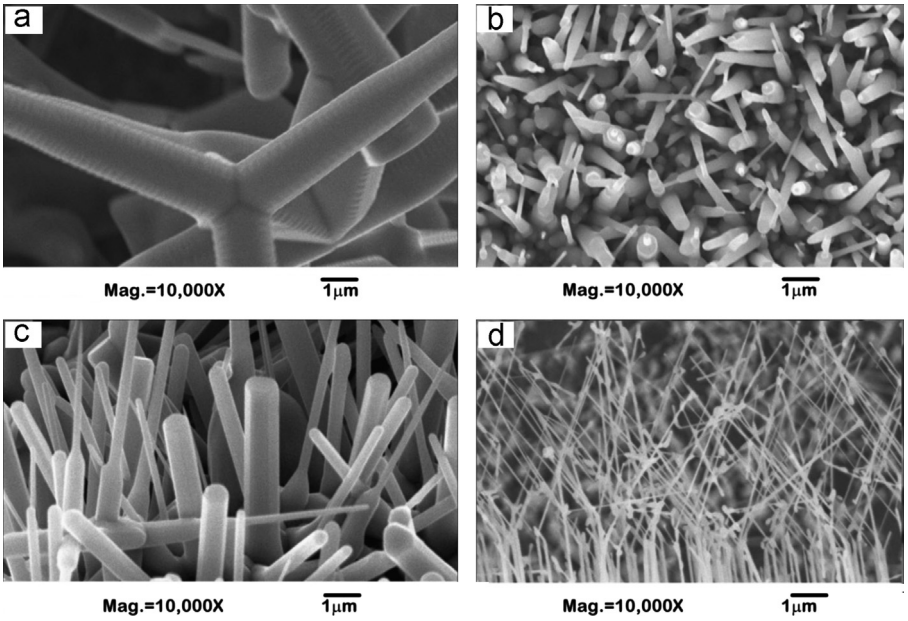

Fig. 1. SEM images of the 1D ZnO nanostructures grown on different substrates: (a) Si (100), (b) Si (111), (c) SiO_2, and (d) sapphire.

900 °C on the morphology of the ZnO nanostructures is clearly observed. The substrate affected the shape and diameter of the 1D ZnO nanostructures, including ZnO tetra-legged with ultra-long legs, 25 μm length and 200 μm diameter which were grown on Si (100), Fig. 1(a). Well-aligned and highly dense ZnO nanorods were obtained when changing substrate from Si (100) to Si (111), Fig. 1(b), where both diameter and length changed; the mean length and diameter are 2 μm and 200 nm respectively. A considerable change in the 1D ZnO nanostructures length and diameters occurred when changing substrate to SiO_2; hexagonal-shaped ZnO nanorods were vertically aligned with a diameter in the range of 200–500 nm and about 3 μm in length. Finally, replacing SiO_2 substrate by sapphire resulted in changing both the shape and size of the grown 1D ZnO nanostructures; ultra thin nanowires with a diameter of about 40 nm were observed; see Fig. 1(d).

Based on the obtained results and under the experimental conditions used in this study, the growth mechanism of 1D ZnO nanostructures occurred via VS, as no metal was used as a catalyst. Hereafter, a reasonable growth mechanism for the formation of 1D ZnO nanostructures was proposed. Basically, the formation of the observed nanostructures can be divided into two stages: nucleation and growth. As the temperature of the furnace reached 900 °C under the continuous flow of N_2, the rising zinc vapor coated the substrate. When oxygen started feeding into the quartz tube, the zinc vapor reacted with oxygen to form ZnO nuclei, with hexagonal bases originating from the center of these nuclei. The nanorods were randomly grown layer by layer on these bases, which seemed to be the roots of the nanorods. These formed ZnO vapors condensed and nucleated in the form of ZnO nanocrystals. As the reactant concentration increased, the ZnO nuclei individually grew along an upward direction in the form of nanorods. The different morphologies may be related most probably to the lattice mismatch between the bases of randomly grown ZnO first nucleus and the type of substrate, which leads to the various obtained shapes (tetra-legged nanorods, nanorods, nanowires, and nanotubes), various diameters and lengths of the final 1D ZnO nanostructures.

3.2. Crystal structure analysis

The 1D ZnO nanostructures obtained via the VS mechanism crystallize within the hexagonal wurtzite crystal structure. The growth rate of the ZnO nanocrystals was affected by the change of the type of substrate, which allowed the development of various shapes and lengths. Thus, the alignment of the 1D ZnO grown tended to be different according to the type of substrate, which means that the intensity of the diffraction peak will vary considerably. Fig. 2 shows typical XRD patterns of ZnO nanostructures grown on Si (100), Si (111), SiO_2 and sapphire substrates via the VS method. All samples showed

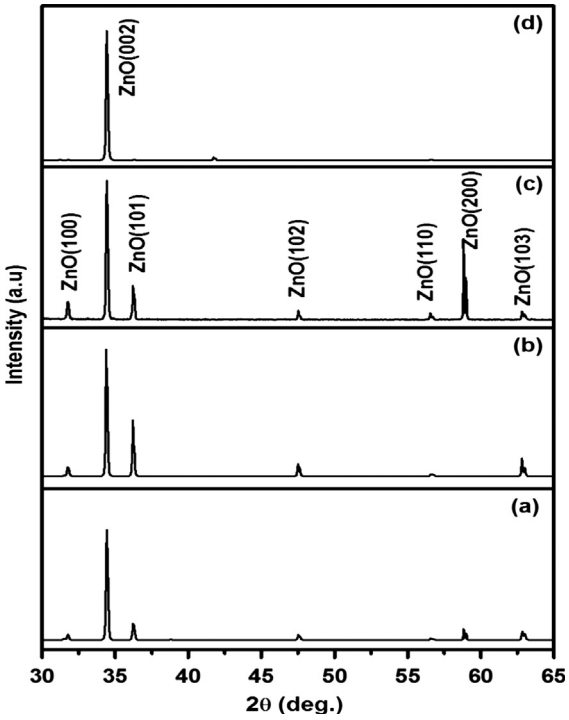

Fig. 2. XRD patterns of the 1D ZnO nanostructures grown on different substrates: (a) Si (100), (b) Si (111), (c) SiO_2, and (d) sapphire.

sharp, highly intense peaks which matched very well with the standard bulk ZnO having a hexagonal crystal structure (JCPDS card no. 800075). The diffraction patterns of the three samples grown on Si (100), Si (111) and SiO_2 were similar. Three pronounced ZnO diffraction peaks with different intensities namely (100), (002), and (101) were observed as well as weak peaks corresponding to the (102), (110), and (103) reflection planes, respectively. Except in the case of ZnO grown on sapphire which showed only one very intense peak (002) all the remaining peaks were not detected, indicating a strong preferred orientation along the (002) direction. Among all the prepared samples, the relatively higher diffraction intensity obtained at (002) plane indicated that the preferred growth orientation was toward the direction of the *c*-axis [23]. Notably, the crystallinity of the fabricated nanostructures was clearly dependent on the type of substrate, which was enhanced by changing the substrate to the sapphire. The full width at half maximum (FWHM) values of the (002) peak for 1D ZnO grown on sapphire and Si (111) were at 0.160° and 0.165°, respectively, which is smaller than that of ZnO grown on Si (100) and SiO_2, indicating that the best crystalline structure was obtained. This configuration was confirmed by the PL measurements of the 1D ZnO nanostructures, which will be discussed in the following section.

3.3. Photoluminescence study

The PL spectra of the ZnO nanostructures grown on Si (100), Si (111), SiO_2 and sapphire are shown in Fig. 3. All

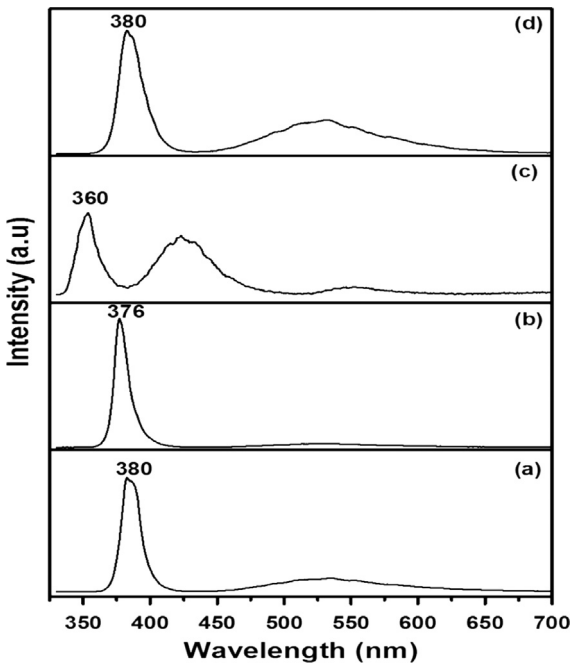

Fig. 3. Room temperature PL spectra of the 1D ZnO nanostructures grown on different substrates: (a) Si (100), (b) Si (111), (c) SiO_2, and (d) sapphire.

samples grown through VS showed two peaks in the PL spectra, a high near-band-edge (NBE) emission at the ultraviolet (UV) region with different intensities, and a broad deep-level emission (DLE) around the green emission. The ZnO nanorods grown on Si (111) substrate showed the highest UV intensity with narrower FWHM and lowest green emission, whereas the remaining ZnO nanostructures showed a high UV intensities and different green emission intensity in the PL spectra. The peak position for the NBE UV emission was the same for the ZnO nanostructures grown on Si (100) and sapphire at 380 nm but with different intensities while it was 376 nm for ZnO nanorods grown on Si (111) and a blue shifted peak at 360 for that grown on SiO_2. This peak was generated by the recombination of the excitons through an exciton–exciton collision process [24].

A broad green emission from ZnO nanostructure was related to sub-band transition, and the nature of the DLE seemed to be intrinsic. Based on available literature, different types of defects related to the PL spectra have been reported [3,8,16,24–28]. The reason for the presence of this peak may be related to the exciton that was bound to structural defects, strain-induced structural defects, incorporation of impurity-induced disorder, or surface defects during the growth process.

The narrow peak with a high-intensity NBE emission, as well as the decrease in the green emission peak (DLE) observed in Fig. 3, resulted from high crystallization. The improvement of crystal quality could cause a high-intensity NBE with very low or no green emission [16]. Thus, the ZnO grown on Si (111) and sapphire showed the best crystallization. As for the green emission, the peak wavelength was around 533 nm for these samples. The difference in the intensity of the peak indicated that the level of defects in the samples was responsible for the recombination of the green luminescence. This finding could be related to the high quantity of surface oxygen vacancies and defects of ZnO, such as Zn vacancy (V_{Zn}). An oxygen vacancy has three possible charge states: neutral oxygen vacancy (VO^{o}), singly ionized oxygen vacancy (VO^{+}), and doubly ionized oxygen vacancy (VO^{++}). The singly ionized oxygen state is known to be unstable, and the transition involving it can be seen as a red emission in PL spectrum. Therefore, oxygen vacancies are either in the neutral or doubly charged states. DLE has been suggested to be related to the defects existing within the samples, including O_2 and Zn vacancies, as well as interstitials and Zn anti-sites [29–35], and results from the recombination of a photo-generated hole with these defects.

Therefore, the difference in the peak intensity can be an indication of the level of defects existing in the samples [32,33,36]. One of the important factors used to compare the optical properties is the UV/DLE ratio [25]. The highest NBE/DLE ratio of ZnO nanostructure grown on Si (111) and sapphire, in addition to the narrow NBE and the decrease in the peak intensity of the green emission, could result from the high crystallinity of the fabricated nanoarchitectures. This is in agreement with the hypothesis that the improvement of the crystal quality can cause a high-intensity NBE with a very low or no green emission. Therefore, the ZnO nanostructures grown on Si (111) and sapphire had the best crystallinity.

3.4. Raman spectroscopy analysis

Raman-scattering spectroscopy (Fig. 4) is an effective technique for estimating the crystallinity of materials. The Raman signals are very sensitive to the crystal structure and to the defects in the crystal structure [16,17,25,37]. The Raman spectrum showed a sharp, strong, and dominant peak at 437 cm^{-1}, known as E_2 (high), the Raman active optical phonon mode (Fig. 4). The E_2 (high) peaks in the as-prepared ZnO nanostructures showed that a blueshift could be attributed to defects and internal strains resulting from different growth directions [16]. This blueshift in the E_2 (high) mode of the wurtzite ZnO crystal structure indicated that the grown ZnO nanostructures were under compressive stress within the *c*-axis-oriented ZnO epilayers [25], to estimate the magnitude of the stress between the 1D ZnO nanostructures and the substrates from the Raman spectra, the blueshift of the wurtzite ZnO crystal lattice under the biaxial compressive stress within *c*-axis can be written according to the following equation [25]:

$$\Delta\omega\ (\mathrm{cm}^{-1}) = 4.4\sigma\ (\mathrm{GPa}). \quad (1)$$

where σ (in the direction of *c*-axis) and $\Delta\omega$ are the stress of 1D ZnO nanostructures in (GPa) and shift of E_2 (high) mode in cm^{-1}, respectively. The frequency of E_2 (high)

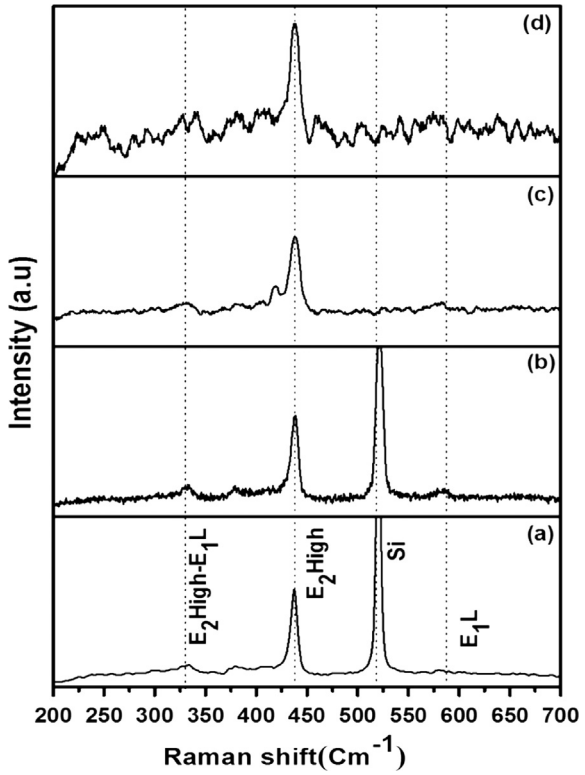

Fig. 4. Typical Raman scattering spectrum of the 1D ZnO nanostructures grown on different substrates: (a) Si (100), (b) Si (111), (c) SiO_2, and (d) sapphire.

Table 1
Variation of shift of E_2 (high) mode ($\Delta\omega$) and stress (σ) with the type of substrate.

Substrate type	E_2 (high) shift (cm^{-1})	Stress (GPa)
Si (100)	1.794	0.41
Si (111)	1.18	0.27
SiO_2	2.33	0.53
Sapphire	1.25	0.28

mode was higher than that in the bulk ZnO for all as-prepared ZnO nanostructures. The E_2 high shift and the stress calculated from Eq. (1) are listed in Table 1.

The E_2 (high) mode blueshift from all as-prepared ZnO nanostructures was very small compared with that of the ZnO bulk [38], i.e. 437 cm^{-1}, owing to the stress relaxation effect from ZnO nanostructures as well as to the fact that all samples were under compressive stress. The values of the blueshift for the ZnO grown listed in Table 1 indicated that the sample grown on Si (111) exhibited fewer internal defects (lower stress).

4. Conclusion

One-dimensional growth of ZnO nanostructures has been observed on four different substrates via thermal evaporation method without using catalysts or additives. Out of the four substrates, we have shown UV emission enhancement for 1D ZnO nanostructure synthesized on Si (111) substrate. Morphological observations showed the formation of 1D ZnO nanostructures with various shapes including nanotetrapods, nanorods, and nanowires having different lengths. Growth mechanisms were proposed for the formation of different morphologies. Detailed structural characterizations confirmed that the formed products were of wurtzite hexagonal phases and were grown along the *c*-axis direction with good crystallinity, depending on the type of substrate. Enhancement in the peaks of the UV emission by changing the substrate could reduce the defects and led to a sharp and strong UV emission at 376 nm at room temperature for the sample that was grown on Si (111). PL spectra showed that the obtained 1D ZnO nanostructures had good crystal quality with excellent optical properties. Moreover, the Raman spectrum showed that the nanorods grown on Si (111) substrate were under less stress, revealing that these nanorods had the best crystal structure with the lowest number of defects.

References

[1] M. Suchea, S. Christoulakis, K. Moschovis, N. Katsarakis, G. Kiriakidis, ZnO transparent thin films for gas sensor applications, Thin Solid Films 515 (2006) 551–554.
[2] O. Lupan, S. Shishiyanu, L. Chow, T. Shishiyanu, Nanostructured zinc oxide gas sensors by successive ionic layer adsorption and reaction method and rapid photothermal processing, Thin Solid Films 516 (2008) 3338–3345.
[3] L. Luo, Y. Zhang, S.S. Mao, L. Lin, Fabrication and characterization of ZnO nanowires based UV photodiodes, Sensors and Actuators A 127 (2006) 201–206.
[4] L.-l. Yang, J.-h. Yang, D.-d. Wang, Y.-j. Zhang, Y.-x. Wang, H.-l. Liu, H.-g. Fan, J.-h. Lang, Photoluminescence and Raman analysis of ZnO nanowires deposited on Si(100) via vapor–liquid–solid process, Physica E 40 (2008) 920–923.
[5] S. Young, L. Ji, T. Fang, S. Chang, Y. Su, X. Du, ZnO ultraviolet photodiodes with Pd contact electrodes, Acta Materialia 55 (2007) 329–333.
[6] N.K. Hassan, M.R. Hashim, N.K. Allam, Low power UV photodetection characteristics of cross-linked ZnO nanorods/nanotetrapods grown on silicon chip, Sensors and Actuators A 192 (2013) 124–129.
[7] X. Kong, X. Sun, X. Li, Y. Li, Catalytic growth of ZnO nanotubes, Materials Chemistry and Physics 82 (2003) 997–1001.
[8] Y. Caglar, M. Caglar, S. Ilican, Microstructural, optical and electrical studies on sol–gel derived ZnO and ZnO:Al films, Current Applied Physics 12 (2012) 963–968.
[9] M.D. Barankin, E. Gonzalez Ii, A.M. Ladwig, R.F. Hicks, Plasma-enhanced chemical vapor deposition of zinc oxide at atmospheric pressure and low temperature, Solar Energy Materials and Solar Cells 91 (2007) 924–930.
[10] A. Umar, S. Lee, Y.S. Lee, K.S. Nahm, Y.B. Hahn, Star-shaped ZnO nanostructures on silicon by cyclic feeding chemical vapor deposition, Journal of Crystal Growth 277 (2005) 479–484.
[11] W.-C. Shih, H.-Y. Su, M.-S. Wu, Deposition of ZnO thin films on SiO_2/Si substrate with Al_2O_3 buffer layer by radio frequency magnetron sputtering for high frequency surface acoustic wave devices, Thin Solid Films 517 (2009) 3378–3381.
[12] W.-C. Shih, R.-C. Huang, Fabrication of high frequency ZnO thin film SAW devices on silicon substrate with a diamond-like carbon

buffer layer using RF magnetron sputtering, Vacuum 83 (2008) 675–678.
[13] J. Shao, W. Dong, D. Li, R. Tao, Z. Deng, T. Wang, G. Meng, S. Zhou, X. Fang, Metal–semiconductor transition in Nb-doped ZnO thin films prepared by pulsed laser deposition, Thin Solid Films 518 (2010) 5288–5291.
[14] M.H. Huang, Y. Wu, H. Feick, N. Tran, E. Weber, P. Yang, Catalytic growth of zinc oxide nanowires by vapor transport, Advanced Materials 13 (2001) 113–116.
[15] E.W. Petersen, E.M. Likovich, K.J. Russell, V. Narayanamurti, Growth of ZnO nanowires catalyzed by size-dependent melting of Au nanoparticles, Nanotechnology 20 (2009) 405603.
[16] A. Umar, S.H. Kim, Y.B. Hahn, Sea-urchin-like ZnO nanostructures on Si by oxidation of Zn metal powders: structural and optical properties, Superlattices Microstructures 39 (2006) 145–152.
[17] A. Umar, E.K. Suh, Y.B. Hahn, Non-catalytic growth of high aspect-ratio ZnO nanowires by thermal evaporation, Solid State Communications 139 (2006) 447–451.
[18] A. Umar, S.H. Kim, E.K. Suh, Y.B. Hahn, Ultraviolet-emitting javelin-like ZnO nanorods by thermal evaporation: growth mechanism, structural and optical properties, Chemical Physics Letters 440 (2007) 110–115.
[19] F. Liu, P.J. Cao, H.R. Zhang, C.M. Shen, Z. Wang, J.Q. Li, H.J. Gao, Well-aligned zinc oxide nanorods and nanowires prepared without catalyst, Journal of Crystal Growth 274 (2005) 126–131.
[20] Y.I. Alivov, Ü. Özgür, S. Doğan, D. Johnstone, V. Avrutin, N. Onojima, C. Liu, J. Xie, Q. Fan, H. Morkoç, P. Ruterana, High efficiency n-ZnO/p-SiC heterostructure photodiodes grown by plasma-assisted molecular-beam epitaxy, Superlattices Microstructures 38 (2005) 439–445.
[21] A. Umar, S.H. Kim, Y.S. Lee, K.S. Nahm, Y.B. Hahn, Catalyst-free large-quantity synthesis of ZnO nanorods by a vapor–solid growth mechanism: structural and optical properties, Journal of Crystal Growth 282 (2005) 131–136.
[22] N.K. Hassan, M.R. Hashim, N.K. Allam, ZnO nano-tetrapod photoanodes for enhanced solar-driven water splitting, Chemical Physics Letters 549 (2012) 62–66.
[23] L. Tang, Y. Tian, Y. Liu, Z. Wang, B. Zhou, One-step solution synthesis of urchin-like ZnO superstructures from ZnO rods, Ceramics International 39 (2012) 2303–2308.
[24] J.H. Zheng, Q. Jiang, J.S. Lian, Synthesis and optical properties of flower-like ZnO nanorods by thermal evaporation method, Applied Surface Science 257 (2011) 5083–5087.
[25] R. Yousefi, A.K. Zak, Growth and characterization of ZnO nanowires grown on the Si(111) and Si(100) substrates: optical properties and biaxial stress of nanowires, Materials Science in Semiconductor Processing 14 (2011) 170–174.
[26] K.M.A. Saron, M.R. Hashim, M.A. Farrukh, Stress control in ZnO films on GaN/Al_2O_3 via wet oxidation of Zn under various temperatures, Applied Surface Science 258 (2012) 5200–5205.
[27] N. Kiomarsipour, R. Shoja Razavi, Hydrothermal synthesis and optical property of scale- and spindle-like ZnO, Ceramics International 39 (2013) 813–818.
[28] Y.-S. Lee, S.-N. Lee, I.-K. Park, Growth of ZnO hemispheres on silicon by a hydrothermal method, Ceramics International 39 (2012) 3043–3048.
[29] T. Ren, H.R. Baker, K.M. Poduska, Optical absorption edge shifts in electrodeposited ZnO thin films, Thin Solid Films 515 (2007) 7976–7983.
[30] A. Janotti, C.G. Van de Walle, Fundamentals of zinc oxide as a semiconductor, Reports on Progress in Physics 72 (2009) 126501.
[31] C.H. Ahn, Y.Y. Kim, D.C. Kim, S.K. Mohanta, H.K. Cho, A comparative analysis of deep level emission in ZnO layers deposited by various methods, Journal of Applied Physics 105 (2009) 013502.
[32] N.E. Hsu, W.K. Hung, Y.F. Chen, Origin of defect emission identified by polarized luminescence from aligned ZnO nanorods, Journal of Applied Physics 96 (2004) 4671.
[33] L. Schmidt-Mende, J.L. MacManus-Driscoll, ZnO—nanostructures, defects, and devices, Materials Today 10 (2007) 40–48.
[34] R. Yousefi, B. Kamaluddin, Dependence of photoluminescence peaks and ZnO nanowires diameter grown on silicon substrates at different temperatures and orientations, Journal of Alloys and Compounds 479 (2009) 11–14.
[35] F.K. Shan, G.X. Liu, W.J. Lee, B.C. Shin, The role of oxygen vacancies in epitaxial-deposited ZnO thin films, Journal of Applied Physics 101 (2007) 053106.
[36] S.-H. Jeong, B.-S. Kim, B.-T. Lee, Photoluminescence dependence of ZnO films grown on Si(100) by radio-frequency magnetron sputtering on the growth ambient, Applied Physics Letters 82 (2003) 2625.
[37] F. Jamali-Sheini, R. Yousefi, K.R. Patil, Surface characterization of Au–ZnO nanowire films, Ceramics International 38 (2012) 6665–6670.
[38] J. Calleja, M. Cardona, Resonant Raman scattering in ZnO, Physical Review B 16 (1977) 3753–3761.